A Study on the Requirements for Fast Active Turbine Tip Clearance Control Systems

Jonathan A. DeCastro
QSS Group, Inc., Cleveland, Ohio

Kevin J. Melcher
Glenn Research Center, Cleveland, Ohio

The NASA STI Program Office . . . in Profile

Since its founding, NASA has been dedicated to the advancement of aeronautics and space science. The NASA Scientific and Technical Information (STI) Program Office plays a key part in helping NASA maintain this important role.

The NASA STI Program Office is operated by Langley Research Center, the Lead Center for NASA's scientific and technical information. The NASA STI Program Office provides access to the NASA STI Database, the largest collection of aeronautical and space science STI in the world. The Program Office is also NASA's institutional mechanism for disseminating the results of its research and development activities. These results are published by NASA in the NASA STI Report Series, which includes the following report types:

- TECHNICAL PUBLICATION. Reports of completed research or a major significant phase of research that present the results of NASA programs and include extensive data or theoretical analysis. Includes compilations of significant scientific and technical data and information deemed to be of continuing reference value. NASA's counterpart of peer-reviewed formal professional papers but has less stringent limitations on manuscript length and extent of graphic presentations.

- TECHNICAL MEMORANDUM. Scientific and technical findings that are preliminary or of specialized interest, e.g., quick release reports, working papers, and bibliographies that contain minimal annotation. Does not contain extensive analysis.

- CONTRACTOR REPORT. Scientific and technical findings by NASA-sponsored contractors and grantees.

- CONFERENCE PUBLICATION. Collected papers from scientific and technical conferences, symposia, seminars, or other meetings sponsored or cosponsored by NASA.

- SPECIAL PUBLICATION. Scientific, technical, or historical information from NASA programs, projects, and missions, often concerned with subjects having substantial public interest.

- TECHNICAL TRANSLATION. English-language translations of foreign scientific and technical material pertinent to NASA's mission.

Specialized services that complement the STI Program Office's diverse offerings include creating custom thesauri, building customized databases, organizing and publishing research results . . . even providing videos.

For more information about the NASA STI Program Office, see the following:

- Access the NASA STI Program Home Page at *http://www.sti.nasa.gov*

- E-mail your question via the Internet to help@sti.nasa.gov

- Fax your question to the NASA Access Help Desk at 301–621–0134

- Telephone the NASA Access Help Desk at 301–621–0390

- Write to:
  NASA Access Help Desk
  NASA Center for AeroSpace Information
  7121 Standard Drive
  Hanover, MD 21076

A Study on the Requirements for Fast Active Turbine Tip Clearance Control Systems

Jonathan A. DeCastro
QSS Group, Inc., Cleveland, Ohio

Kevin J. Melcher
Glenn Research Center, Cleveland, Ohio

National Aeronautics and
Space Administration

Glenn Research Center

July 2004

Acknowledgments

This report contains preliminary findings, subject to revision as analysis proceeds.

Available from

A Study on the Requirements for Fast Active Turbine Tip Clearance Control Systems

Jonathan A. DeCastro
QSS Group, Inc.
Cleveland, Ohio 44135

Kevin J. Melcher
National Aeronautics and Space Administration
Glenn Research Center
Cleveland, Ohio 44135

This paper addresses the requirements of a control system for active turbine tip clearance control in a generic commercial turbofan engine through design and analysis. The control objective is to articulate the shroud in the high pressure turbine section in order to maintain a certain clearance set point given several possible engine transient events. The system must also exhibit reasonable robustness to modeling uncertainties and reasonable noise rejection properties. Two actuators were chosen to fulfill such a requirement, both of which possess different levels of technological readiness: electrohydraulic servovalves and piezoelectric stacks. Identification of design constraints, desired actuator parameters, and actuator limitations are addressed in depth; all of which are intimately tied with the hardware and controller design process. Analytical demonstrations of the performance and robustness characteristics of the two axisymmetric LQG clearance control systems are presented. Takeoff simulation results show that both actuators are capable of maintaining the clearance within acceptable bounds and demonstrate robustness to parameter uncertainty. The present model-based control strategy was employed to demonstrate the tradeoff between performance, control effort, and robustness and to implement optimal state estimation in a noisy engine environment with intent to eliminate ad hoc methods for designing reliable control systems.

Nomenclature

A	state matrix for linear model	F	disturbance input matrix for linear model
$\overline{A}$	transformed state matrix	$\overline{F}$	transformed output matrix
$\overline{A}_c$	controlled partition of $\overline{A}$	F_a	actuator load force
$\overline{A}_r$	residual partition of $\overline{A}$	$\overline{F}_c$	controlled partition of $\overline{F}$
$\overline{A}_{cr}$	residual-to-controlled partition of $\overline{A}$	J	cost function for controller optimization
$\overline{A}_{rc}$	controlled-to-residual partition of $\overline{A}$	K	full state gain
Alt	altitude	K_I	integral state gain
B	input matrix for linear model	K_{amp}	amplifier gain
$\overline{B}$	transformed input matrix	K_{mch}	mechanical gain
$\overline{B}_c$	controlled partition of $\overline{B}$	L	estimator gain
$\overline{B}_r$	residual partition of $\overline{B}$	PLA	engine throttle position
C	output matrix for linear model	Δp_{shd}	shroud pressure gradient
$\overline{C}$	transformed output matrix	Q	observability Gramian
$\overline{C}_c$	controlled partition of $\overline{C}$	S	controllability Gramian
$\overline{C}_r$	residual partition of $\overline{C}$	SFC	specific fuel consumption
D	feedthrough matrix for linear model	T	transformation matrix
EGT	exhaust gas temperature	T_{shd}	shroud temperature
		U	piezoelectric stack voltage

XM	engine Mach number	x_a	actuator position
Y_{33}^E	Young's modulus of piezoelectric actuator	$\tilde{x}_a$	actuator position measurement
c	damping	x_d	combined component deformation
d_{33}	piezoelectric coupling coefficient	w	process noise vector for linear model
e_g	clearance error	y	output vector for linear model
g_{cold}	cold clearance	z	transformed state vector for linear model
g_{min}	minimum measured clearance	z_c	controlled transformed states
k_{eff}	effective stiffness	$\hat{z}_c$	estimated transformed states
k_{fs}	failsafe spring constant	z_I	integral state
k_{stack}	piezoelectric stack stiffness	z_r	residual transformed states
m	shroud mass		
m_{eff}	effective mass	Φ	matrix of eigenvectors
m_{stack}	piezoelectric stack mass	δ_{case}	radial deformation of case
n	number of wafers in piezoelectric stack	δ_{rotor}	radial deformation of rotor assembly
p_a	atmospheric pressure	δ_{shroud}	radial deformation of shroud
p_s	supply pressure	ε	parameter used to maintain nonzero stability margins
u	vector of inputs		
v_1	position measurement noise	ε_{33}	dielectric permittivity
v_2	clearance measurement noise	ρ	material density
x	state vector for linear model		

I. Introduction

This paper presents the results of a study conducted to assess requirements for an active turbine blade tip clearance control system for a large commercial aircraft engine. Blade tip clearance continues to be an issue for concern in gas turbine engines, particularly in the high-pressure turbine (HPT) section.[1-3] During large-magnitude transient events such as takeoff or re-burst, clearance is greatly reduced because the spool speed-up causes the rotor and blades to grow relative to the case and tip shroud creating a "pinch point" (see Figure 1). Immediately following this pinch point, the clearance again increases because of the unavoidable mismatch between the thermal expansion coefficients of the stator and rotor assemblies. In order to eliminate the possibility of rubs occurring at the pinch point, engine manufacturers have introduced a cold build clearance, which inevitably penalizes performance during cruise and over the majority of the flight envelope. More flow is allowed to bypass the blade, thereby decreasing
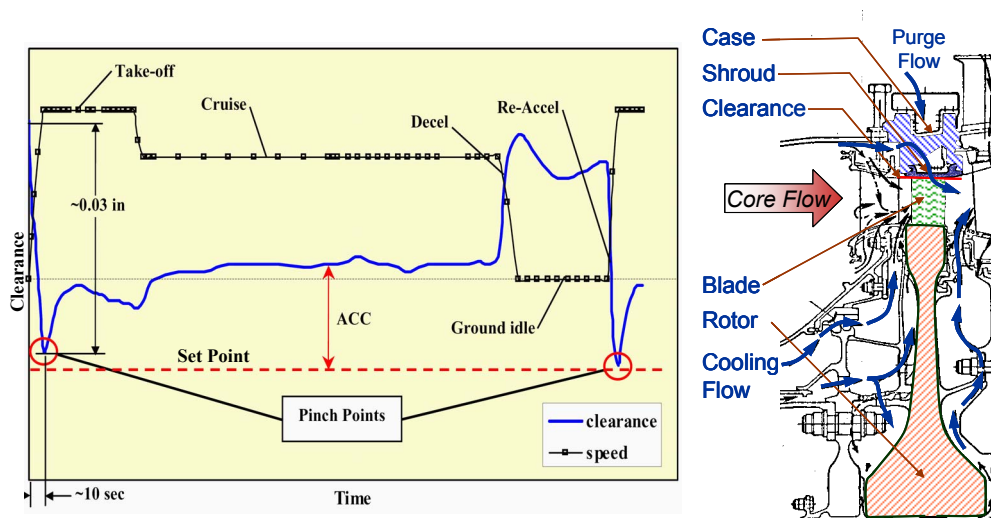

Figure 1: Changes in tip clearance during a notional mission profile[4] and turbine stage cross-section.[1]

specific work and increasing specific fuel consumption (SFC). Likewise, as the turbine's specific work decreases, the engine's controller creates higher fuel burn demands, resulting in increased temperatures and possibly premature maintenance. Degraded or worn turbine blades compound this effect. One indicator of an engine's health state is the exhaust gas temperature (EGT), which must be within an acceptable limit in order for the engine to remain on wing. During takeoff, a significant EGT overshoot is attributable to an increase in clearance, which cannot be mitigated at present.

Improving fuel consumption, increasing engine longevity, and decreasing weight requirements are all goals that can be met though fast active HPT clearance control (FACC). Thermal clearance control systems presently in use in the aircraft industry possess slow response times and thus require conservative, variable clearance set points that are scheduled depending on the potential of re-burst rubs. Although mechanical concepts were first introduced nearly 40 years ago,[3] fast active clearance control has recently experienced a renewed emphasis in light of meeting the aforementioned performance requirements. In order to implement a control system, accurate plant models of the turbine section[5,6] and experimental validation of the entire system are needed.[7] In order to be acceptable, the control system must maintain a constant clearance setting over all operating points, while providing rub-free (failsafe) performance using actuation that requires minimal power consumption and a small geometrical footprint. Depending on efficiency tradeoffs, these fast systems will either work in conjunction with or replace existing thermal control systems. Many actuators and sensors are available that can provide the precise control that is sought, but an analytical study is necessary to determine if the candidate systems meet the design constraints.

This paper serves to address the key requirements for the realization of a fast active clearance control system through a trade study given the dynamic transients of a generic turbofan engine. The document is divided into five sections. Section II deals with design requirements and constraints for FACC hardware such as force, stroke, and failsafe requirements; and addresses control and estimation needs. The specific actuators investigated herein are also presented. Section III discusses development of a model-based servohydraulic actuator control system and estimator structure. Simulation results on a nonlinear actuator model containing saturation limits and nonlinear fluid dynamics are presented as well as an assessment of the system's robustness. Section IV details the design and selection of a piezoelectric actuator for the target application, controller design, and simulation results and robustness assessment. The paper concludes with a summary of the present findings and future work activities.

II. Design Requirements and Constraints

A summary of the specific requirements and environmental and geometrical characteristics inside of the case (pressure vessel) are given in Table 1. The specifications of the target test rig at NASA Glenn Research Center (GRC) developed by Lattime and Steinetz[7] are compared with those for a large generic commercial engine. Because FACC systems are intended to be incorporated into future engine design cycles, the exact requirements and benefits of clearance control cannot be determined *a priori*. Therefore, the values reported in the table are based on the current state-of-the-art with additional margins factored in for broader applicability. It should be noted that the number of sensors is far fewer than the number of actuators and thus a one-to-one correspondence between actuators and sensors does not exist. This imposes an inherent difficulty for measurement of distributed clearance, as will be discussed later. The force requirement is based on the maximum pressure differential across the shroud, while the displacement criterion is based on the typical combined deformations $x_d(t)$ of turbine components. This quantity is related to the clearance gap $g(t)$ as follows:

$$
\begin{aligned}
g(t) &= g_{cold} + \delta_{shroud}(t) + \delta_{case}(t) - \delta_{rotor}(t) \\
&= g_{cold} + \delta_{case}(t) - \delta_{rotor}(t) - x_a(t) \\
&= x_d(t) - x_a(t)
\end{aligned}
\tag{1}
$$

where g_{cold} is the cold clearance or bias gap and $\delta_{case}(t)$, $\delta_{shroud}(t)$, and $\delta_{rotor}(t)$ are the outward thermal and mechanical deformations of the case, shroud, and rotor assembly relative to the cold clearance, respectively. With actuation, $\delta_{shroud}(t)$ in Eq. (1) is replaced by the negative actuator position $-x_a(t)$ because the mechanical properties of the shroud supports are replaced by the actuator.

As outlined earlier, the benefits of active clearance control are to reduce SFC and EGT overshoot in order to improve engine longevity and improve fuel savings. As reported in Wiseman and Guo,[2] a clearance reduction of 10 mils results in an overall approximate SFC improvement of 1% over the mission. According to Lattime and

Table 1: Specifications and requirements for FACC.

	Large Commercial Aircraft Engine	NASA FACC Rig[7]
Displacement capability	0.1 in	0.1 in
Force capability	2200 lbf	2200 lbf
Max. pressure differential across shroud	150 psi	120 psi
Number of actuators	20	9
Number of sensors	3 or more	6
Hydraulic pressure	4000 psi	4700 psi
Headroom between case and shroud	1 – 2 in	n/a
Temperature inside case	> 1300°F	1500°F
Temperature outside case	600°F	ambient

Steinetz,[1] a 10-mil improvement is projected to save the airline industry $160M per year if FACC is applied across the entire fleet. Such a reduction roughly translates into a peak takeoff EGT reduction of 18°F which increases the engine's time-on-wing.[2] In order to achieve these clearances in the presence of asymmetric (out-of-roundness) events, it is clear that distributed sensing and actuation is required to guarantee a certain circumferential clearance. However, there are inherent difficulties associated with non-collocation of actuators and sensors, so the present study only addresses *axisymmetric* clearance control. With this scheme, a certain minimum clearance is calculated based on several annular measurements and a single position command is provided to each actuator. A conservative clearance set point must therefore be maintained in order to allow for unobservable out-of-roundness effects as well as clearance tracking errors during transients. As a target for the present study, a clearance set point of 5 mils was chosen over the entirety of the mission profile, with maximum allowable tracking errors of less than 2 mils. For the sake of completeness, the FACC system should be validated with step displacement command tracking, step force disturbance rejection, and clearance tracking with a representative takeoff transient event composed of force and displacement transients. The step inputs are intended to approximately represent events such as engine start-up or sudden asymmetric events, such as gyroscopic engine motion.

The engine is a harsh environment for precise shroud positioning control because the system may be exposed to parameter drifts due to environmental factors as well as periodic or noisy exogenous forces. Parameter uncertainty is a phenomenon that may arise from model inaccuracies, neglected dynamics, nonlinearities, or temperature- and pressure-induced parameter variations. If, for example, the properties of the actuator are significantly affected by temperature variations, performance may degrade beyond acceptable limits. Careful attention must be paid to validating the control system in the presence of such parameter shifts. Disturbances may enter into the system as either process noise or measurement noise. Possible sources of process disturbances include excitation of the shroud due to gas path turbulence, *N*-per-rev blade passage excitations, or vibrations of the actuator's support structure. The influence of these disturbances is dependent on the properties of the actuator, e.g. its stiffness and mass, but can be mitigated if an estimator and controller are appropriately designed. Measurement noise can arise from gas path impurities, transmission cable EMI, or target surface fouling, but the intensity of the noise depends on the type of sensor used and the operating environment. Capacitance probes are the most flight-ready of the clearance sensors, but they suffer from noise corruption induced by gas path ionization.[8] Microwave probes, on the other hand, are less advanced but offer the best performance of all the clearance sensors due to their low susceptibility to gas path noise. In either case, noise-free noise signal transmission cannot be guaranteed in such a harsh environment.

Description of Actuator Candidates

The present study is concerned with examining the closed loop response of two types of actuators that reflect the goals of the Ultra-Efficient Engine Technologies (UEET) program at NASA GRC.[6] It is intended to use an electrohydraulic servovalve actuator as a first-generation FACC design on the NASA test rig. Electrohydraulic servovalves possesses high-performance, low-maintenance characteristics, making this form of actuation a more flight-ready technology. These systems would utilize the onboard fuel as the working fluid to actuate a hydraulic ram coupled to the shroud hangar. Servovalves manufactured by MOOG, Inc.[9] can withstand temperatures above 600°F, which is marginally acceptable for placement on the exterior of the case. Concern has been addressed that, even with secondary seals in place, penetration of the pressure vessel from outside the case may cause a leak path that can significantly detract from the overall benefit of FACC.[1] The actuators may be placed inside the case to eliminate this potential leakage, however, the hardware's size and thermal limitations (e.g. coking of the working fluid) make this solution a difficult one to realize.

The second type of actuator investigated here, though intended as a longer-term solution, is based on smart material technologies. At present, there is a drive to introduce and eventually replace conventional engine actuation hardware with smart materials in order to reduce the overall size and weight stack-up on the engine, with the goal of transitioning to a completely electrically-actuated engine. In this study, piezoelectric actuators were examined due to their favorable linearity and energy density. However, there are several challenges that hinder implementation of these devices. For one, the strain capability of piezo-ceramic stacks is limited, having strains of less than 2.0 mils/in.[10] This is a concern for minimizing the package size and weight; however recent developments in *piezo-crystal* stack technology have advanced strain capability to above 10 mils/in.[11,12] As will be shown, stack force capability is far greater than the loads seen by the actuator, so it is possible to employ a displacement amplification mechanism to satisfy the displacement criterion. For another, the temperature handling capability of the PZT ceramic material, limited by the depoling (Curie) temperature, is typically less than 400°F. Although piezoelectric devices were chosen for the present study, other energy-dense active material candidates show promise for high-displacement operation, but are faced with other unique implementation challenges. One such technology is shape memory alloys (Nitinol), which possess strain capabilities of 60 mils/in.[10] and have already been proposed as a viable clearance control method.[13] The drawbacks with those actuators are in their highly hysteretic and temperature-dependent characteristics. Electrostrictive polymers (P[VDF – TrFE]) is another energy-dense material that is capable of 40 mils/in but, as with shape memory alloys, these are hindered by the nonlinear electromechanical coupling.[10]

Failsafe Requirements

Because the shroud hangar experiences pressure load forces acting radially inward, the proposed system must employ a restoring spring to prevent rubs from occurring. A mechanical stop would be used to establish a preload, which may be adjusted to manually in order to limit the outward motion to maintain a conservative clearance and thus allow for continued operation at reduced engine performance. The spring constant and static preload are determined by the maximum force acting on the shroud at the minimum clearance point (which are roughly coincident). Based on a 2200 lbf force and a spring constant of 15,000 lbf/in, a preload of 1530 lbf is required for the failsafe mechanism to operate correctly. With the failsafe mechanism in place, the actuator must displace against the spring force at high-clearance conditions such as ground idle to maintain the set point. Unfortunately, as blade tips erode with time, the actuator must provide a greater force in order to make up for the additional cold clearance gap.

III. Control Loop Approach

In order to satisfy the requirements and constraints set forth in the previous section, it is desired to utilize control laws that exhibit reasonable performance and robustness. The block diagram in Fig. 2 shows the control loop architecture used presently for clearance control. From a controls standpoint, the engine can be thought of as a *disturbance generator* due to the weak feedback between clearance and engine states. The FACC system enters in as a clearance regulator with a set point of 5 mils and utilizes both position and clearance measurements. Actuator
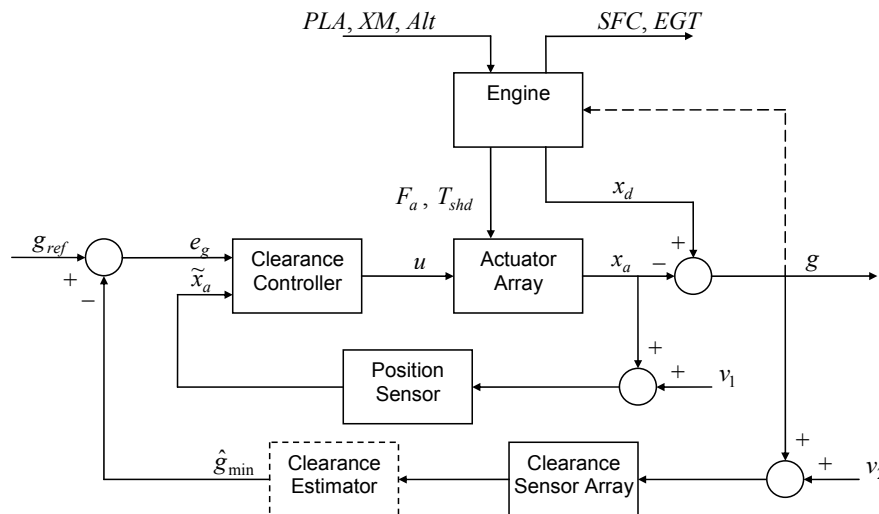

Figure 2: FACC control loop. The dashed arrow indicates the "slow" coupling between clearance and the engine states. Design of the clearance estimator is not treated in this study.

measurements are used in the design for two reasons. For one, optimal multivariable control laws require the actuator states to be observable, which clearance measurements cannot provide due to the unknown component deformations. If these deformations are estimated using only a model, errors in that model will be "absorbed" by the actuator position estimate, undoubtedly resulting in sub-optimal performance. For another, several strategically-placed clearance sensors are used to ascertain an approximate minimum clearance estimate, which is then used to feedback a clearance error. Because the number of sensors is in general far fewer than the number of actuators, larger-than-expected clearance errors may be introduced at locations where clearance is not measured. The design of a high fidelity *clearance estimator* to detect asymmetric clearance variations (refer to Fig. 2) would allow an estimated error signal to be calculated at each driving point and may involve using either a detailed turbine section model with circumferentially-resolved dynamics or a simple n^{th}-order polynomial to interpolate between sensors. The clearance estimator's design is a topic that will be left for future work.
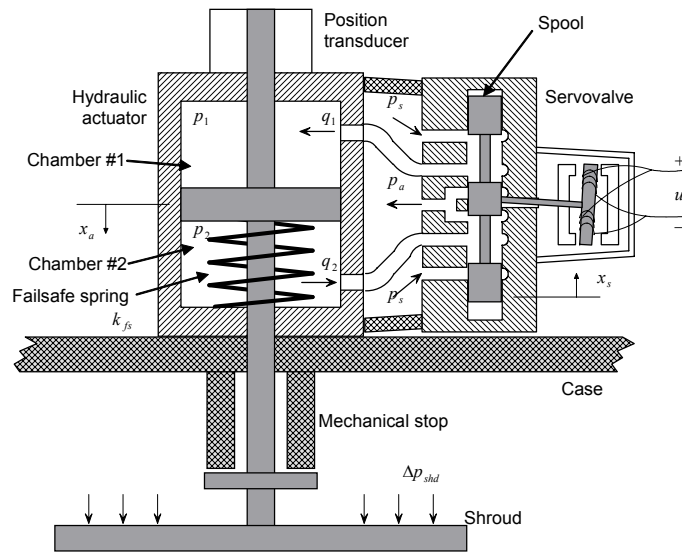
To summarize, the objectives for FACC actuation and control in a large turbofan engine are as follows:

- Possess a stroke length of 0.1 in and a force capability of 2200 lbf.
- Maintain clearance tracking errors to within 2 mils with zero steady-state error when commanded a transient takeoff disturbance profile, assuming a set point of 5 mils.
- Exhibit acceptable performance and stability robustness to parameter variations and nonlinearities.
- Minimize power consumption.

To meet the above objectives, a linear quadratic regulator (LQR) control law was developed in this study to optimally control clearance while respecting the control effort demands of the actuator. Two features were included to improve performance: an integral state and a Kalman estimator. Quite simply, the integral state is used to drive the steady-state clearance error to zero in a finite amount of time. To account for system noise, a Kalman filter estimator is used to optimally reject such stochastic disturbances. When combined, the LQR control law and Kalman estimator form an optimal control law known as a linear quadratic Gaussian (LQG) controller. This control strategy was chosen over classical proportional-plus-integral (PI) control techniques because: 1) LQR may satisfy the aforementioned performance constraints while limiting the control effort, thereby eliminating *ad hoc* approaches to controller design; 2) process and measurement noise may be rejected by means of the Kalman estimator; and 3) this methodology may be extended to include adaptive techniques such as model predictive control (in order to guarantee avoidance of a certain minimum clearance or maximum control effort saturation limits).

IV. Design and Analysis of a Servohydraulic Control System

As discussed in the Section II, the electrohydraulic servovalve actuator was designed as a near-term solution for fulfillment of FACC. Figure 3 shows a conceptual drawing of the system's mechanical operation with case penetration. For actuator motion to occur in the positive *x*-direction, fluid must be supplied to chamber #1, which requires that the valve move in the positive x_s-direction. The spool's movement allows for simultaneous pressurization of chamber #1 (from the supply pressure p_s) and de-pressurization of chamber #2 to the atmosphere (p_a). The failsafe spring and shroud seal damping are schematically represented by the spring constant k_{fs} and damping c, respectively.

A model was developed for a generic two-stage servovalve with mechanical feedback, actuator ram, and shroud hangar. The model consists of six states: valve current *i*, valve spool position x_s, chamber #1 pressure p_1, chamber #2 pressure p_2, actuator velocity $\dot{x}_a$, and actuator position x_a. The model development was adapted from Ref. 14 and the derivation specific to this system is given in the Appendix.

Results presented herein are specific to two servovalve models: MOOG G761-3001 and MOOG 260-0040, whose parameters are given

Figure 3: Concept schematic of an electrohydraulic servovalve actuation system.

Table 2: Parameters used for the servohydraulic actuator model.[9]

	MOOG G761-3001	MOOG 260-0040
Rated flow at 1000 psi	1.0 gpm	1.79 gpm
Rated current I_r	40 mA	50 mA
Max. supply pressure	4500 psi	3000 psi
Coil resistance R_c	80 Ω	40 Ω
Coil inductance L_c	0.22 H	0.13 H
Leakage flow at 3000 psi	0.31 gpm	0.12 gpm
Time constant τ	1.8 ms	1.5 ms

in Table 2. These servovalves were chosen because they exhibit distinctly different performance characteristics from one another, as will be illustrated in the forthcoming analysis. The two valves also present an interesting design tradeoff due to the capabilities of the hardware. Namely, the G761 has a rated pressure of 4500 psi, which requires the actuator piston diameter to be 0.96 inches in order to generate 2200 lbf. The servovalve's weight is 2.4 lb per valve, or 58 lb for 20 valves around the circumference as suggested in Table 1. In contrast, the 260 servovalve is rated at 3000 psi, requiring a piston diameter of 1.17 inches, slightly larger than that required for the, but the valve's weight is 0.68 lb (14 lb for full-circumferential control), significantly lower than that for the G761. Note that weight variations in the accommodating hardware are not considered here.

Controller Design

A state space description of the servosystem was achieved by combining the state space matrices of Eqs. (A.11) to (A.14) in the Appendix. These equations, when corrupted by position measurement noise v_1 and process noise w are

$$\dot{x} = Ax + Bu + Fw$$
$$y = Cx + Du + v_1 \tag{2}$$

where

$$x = \{x_a \quad \dot{x}_a \quad p_1 \quad p_2 \quad x_s \quad i\}^T \tag{3}$$

$D = 0$, $y = x_a$, and the superscript T is the transpose operator.

Early in the design process, it was discovered that the state matrix was poorly conditioned, which diminished the system's controllability and observability characteristics. The states were transformed by obtaining a joint Gramian Σ composed of the singular values of the system. The transformation matrix T must satisfy the joint relationship[15]

$$\Sigma = TST^T = T^{-T}QT^{-1} \tag{4}$$

where S is the controllability Gramian and Q is the observability Gramian. The transformed system was placed into modal canonical form by multiplying the original states by a matrix Φ consisting of the system's eigenvectors. The following state space representation is obtained: [15]

$$\dot{z} = T\Phi A\Phi^{-1}T^{-1}z + T\Phi Bu + T\Phi Fw = \bar{A}z + \bar{B}u + \bar{F}w$$
$$y = C\Phi^{-1}T^{-1}z + Du + v_1 = \bar{C}z + Du + v_1 \tag{5}$$

And the transformed states are $z = T\Phi x$.

When possible, it is desirable to reduce the model's order while retaining essential dynamics of the plant to prevent designing a controller that is unnecessarily complex for implementation. Those states associated with the lowest diagonal singular values in the joint Gramian Σ are the least controllable and observable and should be the first to be eliminated. Of the six transformed states in the present model, three were eliminated. The state vector is

partitioned according to the states to be controlled z_c and residual states to remain uncontrolled z_r such that $z = \{z_c \quad z_r\}^T$. The state matrices are partitioned as $\overline{A} = \begin{bmatrix} \overline{A}_c & \overline{A}_{cr} \\ \overline{A}_{rc} & \overline{A}_r \end{bmatrix}$, $\overline{B} = \begin{bmatrix} \overline{B}_c \\ \overline{B}_r \end{bmatrix}$, and $\overline{C} = \begin{bmatrix} \overline{C}_c & \overline{C}_r \end{bmatrix}$.

In fulfillment of the design objectives, the LQG control law was implemented. Not only is the LQR method attractive for its consideration of control effort, but it guarantees linear stability because it is optimal in the H_2 sense and hence is a departure from the trial-and-error design procedures associated with classical PI controllers. In fact, preliminary results with a PI controller showed that several iterations were needed to obtain a set of linearly stable PI gains, which needed further iteration to be stable in the nonlinear environment. The transformed, reduced order state equation (Eq. (5)) was augmented to include an integral state by writing

$$
\begin{Bmatrix} \dot{z}_I \\ \dot{z}_c \end{Bmatrix} = \begin{bmatrix} -\varepsilon & \overline{C}_c \\ 0 & \overline{A}_c \end{bmatrix} \begin{Bmatrix} z_I \\ z_c \end{Bmatrix} + \begin{bmatrix} 0 \\ \overline{B}_c \end{bmatrix} u + \begin{bmatrix} 0 \\ F_c \end{bmatrix} w - \begin{bmatrix} 1 \\ 0 \end{bmatrix} r
$$
$$
y = \begin{bmatrix} 0 & \overline{C}_c \end{bmatrix} \begin{Bmatrix} z_I \\ z_c \end{Bmatrix} + Du + v_1
$$

(6)

where z_I is the integral state and $r = g_{ref}$ in the present design. The parameter ε is used here to maintain nonzero stability margins on the integral state. The LQR controller must minimize the cost function J given by

$$
J = \int_0^\infty \left[\begin{Bmatrix} z_I(t) & z_c^T(t) \end{Bmatrix} Q_1 \begin{Bmatrix} z_I(t) \\ z_c(t) \end{Bmatrix} + u^T(t) Q_2 u(t) \right] dt
$$

(7)

It is common practice to choose the state weight Q_1 such that the ARE minimizes the output error (position in this context), thus the lower-right entry of Q_1 was chosen as $\overline{C}_c^T \overline{C}_c$ and the upper-left as 0.1. The control effort weight Q_2 is the design variable that will be used to illustrate the weight trade off in the subsequent sections.

The state estimates are obtained by combining the reduced order linear model and the residual between the noisy measurement $y(t)$ and the model output $\overline{C}_c \hat{z}_c(t)$ as follows:

$$
\dot{\hat{z}}_c(t) = \overline{A}_c \hat{z}_c(t) + \overline{B}_c u(t) + L\left[y(t) - \overline{C}_c \hat{z}_c(t) \right]
$$

(8)

Kalman filter theory is employed to find the estimator gain L that optimally rejects measurement and process noise, assuming that the noise is white and unbiased as described in detail in Ref. 16.

In the present system, the force disturbance noise and command voltage noise are approximations based on the author's intuition, and were assigned standard deviations of 100 lbf and 1 mV, respectively. The force disturbance noise is an estimated sum of the quasi-stochastic phenomena acting on the shroud assembly (e.g. turbulence, vibrations), while the command signal noise constitutes any transmission effects that may corrupt the actuator command signal such as cable EMI. The measurement noise standard deviation of 1×10^{-6} inches was estimated based on a survey of SNR values reported by several Linear Variable Differential Transformer (LVDT) manufacturers. Using the estimated states, the full state PI control law is:

$$
u = -K\hat{z}_c - K_I z_I
$$

(9)

The controller gain K is obtained by solving an algebraic Riccati equation (ARE) derived from the cost function in Eq. (7).[16] It should be noted that the control/estimation structure and plant model was designed and implemented in the MATLAB/Simulink environment.

Results and Discussion

To examine the FACC system's step response capabilities, step inputs were fed into the combined deformation x_d and pressure load on the actuator F_a. Based on prior studies, it was found that clearance tracking capabilities

due to a transient force alone was correlated to the system's settling time and less correlated to overshoot. Trade curves between clearance settling time and normalized control effort for both step disturbance inputs are shown in Fig. 4. For these results, a zero order hold with a sample rate of 50 Hz was applied to the plant in order to design the compensator, which is representative of the typical update rate of newer commercial FADEC flight hardware. As can be seen in the figure, both valves are capable of adequate settling times, but each possess different command voltage demands. The discrepancy exists because the available supply pressure differs for both valves and thus the required actuator area is different for both: smaller actuator areas result in larger actuator velocities. The valve's weight generally increases as pressure capability increases, so it is important to consider both control effort and valve weight for control hardware design and selection. It should be noted, however, that the command power requirements of the servovalve may be much lower than the pumping power required to pressurize the hydraulic actuator and therefore it may not make sense to optimize against control effort.

The system was tested next with a transient clearance takeoff event, which is roughly equivalent to a ramp in x_d from 0.05 inches to zero at a rate of -0.010 in/sec coincident with a force ramp from zero to 2000 lbf at a rate of 375 lbf/sec.[7] For a full description of the clearance transient phenomena specific to this application, the reader is referred to Kypuros and Melcher.[5] The trade curves shown in Fig. 5 illustrate the effects on tracking capability with a 5-mil clearance command. The values for Q_2 that violate the 2-mil tracking error criterion are shown, which correspond to larger control effort costs and faster settling times. As reflected in the step responses, the 260 maintains smaller clearance tracking errors for given values of Q_2.

The simulated performance of the control system was validated with the detailed nonlinear model developed in the Appendix. In the simulation, saturation limits placed on the spool position were dictated by the rated current of ±40 mA, actuator position saturation limits were set to +0.1 / -0.005 inches, and the Coulomb damping force was assigned a value of 200 lbf. The step responses shown in Fig. 6 are for the 260 valve with $Q_2 = 2.8 \times 10^{-6}$. Here, Q_2 is chosen to strike a balance between fast response and favorable robustness properties in addition to maintaining small control efforts. As Q_2 is reduced to improve performance, the system's stability margins decrease, as indicated by the fact that simulated responses with Q_2 values below 1.5×10^{-7} resulted in limit cycling. As can be seen in the figure, the linear and nonlinear results coincide quite well in response to a step in x_d, but with small transient errors. Due to limitations of the linear model, the force disturbance responses reveal that the nonlinear simulation tracks slower than the linear case and with greater overshoot.

Using the controller choice from Fig. 6, several parameters were varied independently in order to assess the robustness of the overall system. For this evaluation, noise disturbance variances were set to the design values reported earlier. Both takeoff transient and step disturbance inputs (with magnitudes in Fig. 6) were utilized to exercise the simulation. Parameters that were tested included the hydraulic fluid's bulk modulus, actuator mass, actuator damping, coil resistance, coil inductance, piston area, and supply pressure. Of the seven parameters, only the resistance, area, and pressure had a significant effect on the response. For all parameters except supply pressure, tracking errors were nearly unaffected for large increases from nominal. However, when decreased, the responses demonstrated greater oscillatory behavior and unacceptable overshoot, which entered into a limit cycle if further
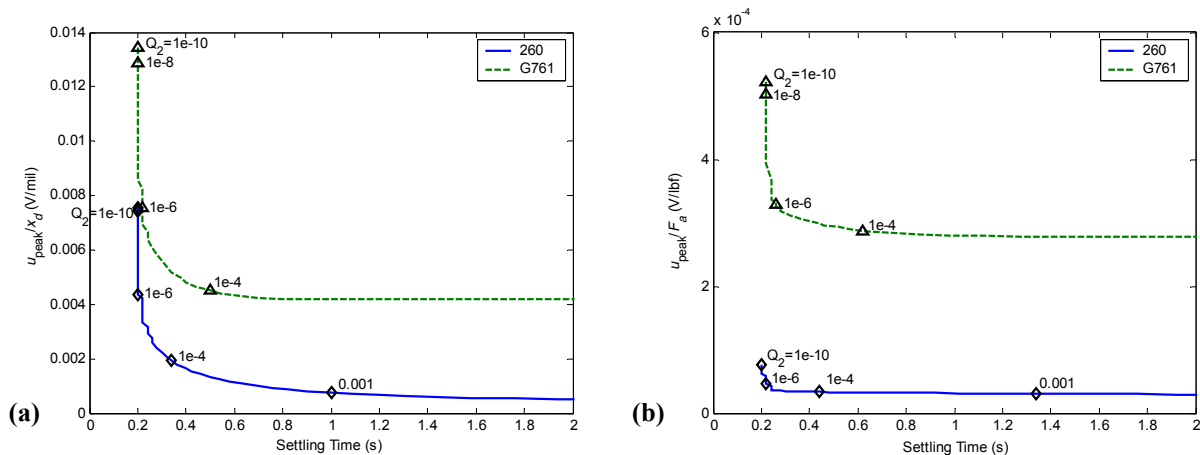

Figure 4: Servohydraulic actuator step response trade curves as functions of Q_2: (a) x_d disturbance, (b) F_a disturbance.

reduced. In particular, the values at which the 2-mil criterion was violated corresponded to 48% and 77% of the nominal resistance and piston area respectively, while the values at which the system began to limit cycle corresponded to 48% and 61%, respectively. In an actual flight environment, uncertainties in piston area are not anticipated to be problematic, but uncertainties in coil resistance may possibly arise from temperature fluctuations in proximity to the servovalve. Reductions in the supply pressure did not cause limit cycling as the other parameters did, but instead significantly influenced the system's robust performance. When the supply pressure was reduced to 78% of the original value, the clearance tracking

Figure 5: Servohydraulic actuator takeoff transient response trade curves as functions of Q_2.

errors became greater than 2-mils. The loss of authority was confirmed by the observation that the control current reached its limit, which caused a disruption in the state estimation error. When the supply pressure was reduced close to zero, however, it was observed that blade rub-ins did not occur during the course of the transient, verifying the operability of the failsafe mechanism with little authority present.

Although simulation results are promising, in order to implement the control system further improvements must be made in order to realize better tolerance to faults such as, e.g., a significant drop-off in supply pressure. In addition to this, servohydraulic actuators possess practical drawbacks that may further hinder implementation. For one, the servohydraulic actuator will introduce a large amount of weight on the engine that may compromise the benefits of FACC. For another, because the hardware has inherent thermal and size limitations, it is expected that these systems will not be able to be placed inside the case. Thus, in order to access the shroud, the actuator mechanism must penetrate the pressure vessel, introducing a potential leak path.

V.   Design and Analysis of a Piezoelectric Control System

To address the shortcomings of conventional technology for FACC, piezoelectric actuation was investigated as an alternative candidate. Piezoelectric actuators can be sized to fit within the space between the case and the shroud given that they are cooled sufficiently to avoid depolarization. Utilizing the full potential of the material, it can be used as a sensoriactuator; i.e. actuators that can self-transduce their position, eliminating the need for the additional position sensor component. If provisions are made to estimate the time-varying stack capacitance, one then may compute a high-accuracy position measurement. One concept for shroud articulation using a piezoelectric stack is shown in Fig. 7. Because the piezoelectric wafers separate under tensile forces, the stack must be placed in
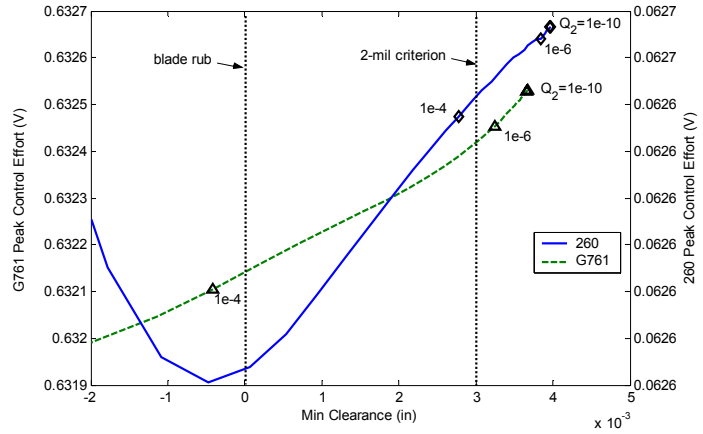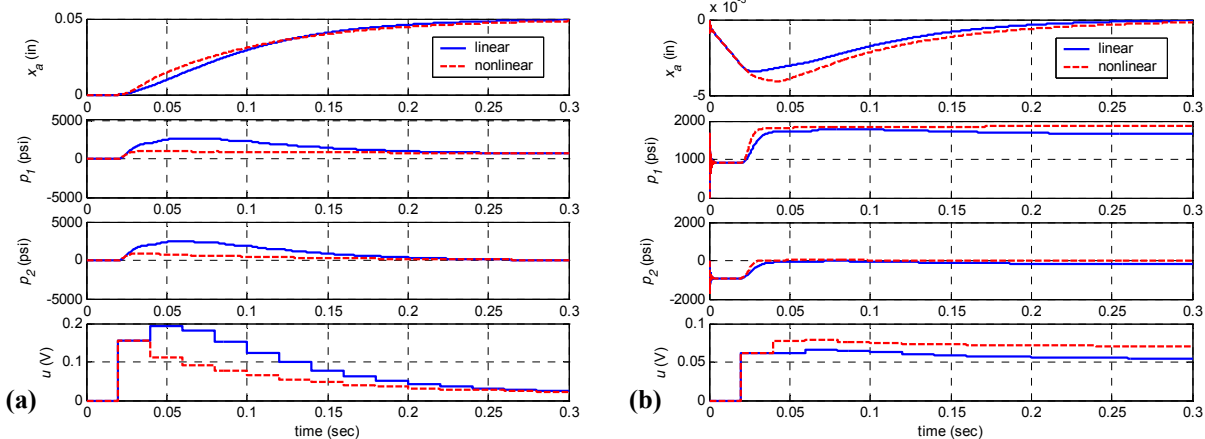

Figure 6: Linear and nonlinear step responses for MOOG 260-0040 and $Q_2 = 2.8 \times 10^{-6}$: (a) x_d = 50 mils, (b) F_a = 2000 lbf.

compression as shown with the failsafe spring pre-loaded to resist motion into the blades. Amplification of the displacement may be accomplished by use of a lever arm or a hydraulic amplifier if the actuator possesses a blocked force greater than the requirement, which is used in several applications.[11,17] Energy conservation laws dictate that a gain in displacement is always penalized by an attenuation in force. Using this premise, one can "tune" the amplifier gain to ensure that the actuator is at its maximum mechanical efficiency, otherwise known as *impedance matching*, which is achieved at one-half of the free (unloaded) displacement and one-half of the blocked force.

A model for the amplified piezoelectric stack with mechanical gain K_{mch} is a modified form of the constitutive equation,[18] which is embodied in the following expression:
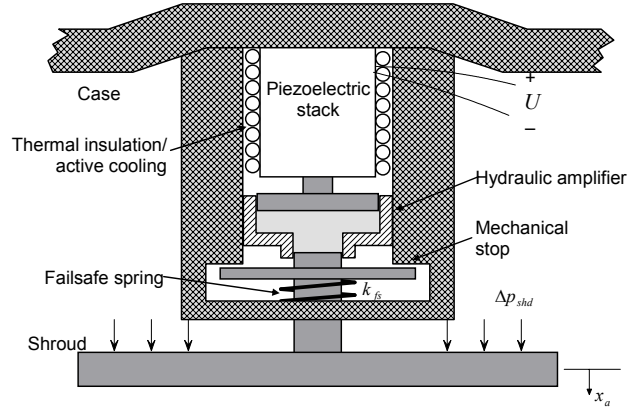

Figure 7: Concept schematic of a piezoelectric actuation system with mechanical amplification.

$$\frac{n d_{33} k_{stack}}{K_{mch}} U + F_a = k_{eff} x_a + c_{eff} \dot{x}_a + m_{eff} \ddot{x}_a \tag{10}$$

where $k_{eff} = k_{stack}/K_{mch}^2 + k_{fs}$, $c_{eff} = c_{stack}/K_{mch}^2 + c$, and $m_{eff} = m_{stack}/K_{mch}^2 + m$. The electromechanical coupling depends on the number of wafers n in the stack and the piezoelectric coupling coefficient d_{33}. The voltage amplifier was modeled as a low pass filter from the input voltage u to the amplified (stack) voltage U accordingly:

$$K_{amp} u = \tau \dot{U} + U \tag{11}$$

where τ is determined from the stack's capacitance and the amplifier's rated current and voltage. Eqs. (10) and (11), along with a state equation assigning $\dot{x}_a$ a new state variable, constitute the state space piezoelectric model and may be readily cast in the same form as Eq. (2).

Single crystal relaxor ferroelastics (PMN-PT and PZN-PT) are new materials that possess strain capabilities well above 1% and hence are the most promising piezoelectric candidates from an actuator weight and profile minimization standpoint. These materials are currently in the development phase, so the actuator dimensions and wafer thickness are calculated based on the requirements of the present study (see Table 1). The actuator parameters for the PZN-PT material for a stack configuration are shown Table 3. To achieve maximum mechanical efficiency, the stack and mechanical amplifier must be sized to output twice the required free displacement and twice the required blocked force. Using the steady-state form of Eq. (10) and the values from Table 3, the 0.2-in free displacement criterion may be satisfied with a 1-inch actuator length by setting $K_{mch} = 20$. To obtain a blocked force of 4400 lbf, Eq. (10) is used again to compute an actuator stiffness of $k_{stack} = 8.8 \times 10^6$ lbf/in which, through the simple stress-strain relationship, requires an actuator area of 7.28 in². For the present design, it should be noted that the total weight is nearly 43 lb if 20 stacks are used for full-circumferential control.
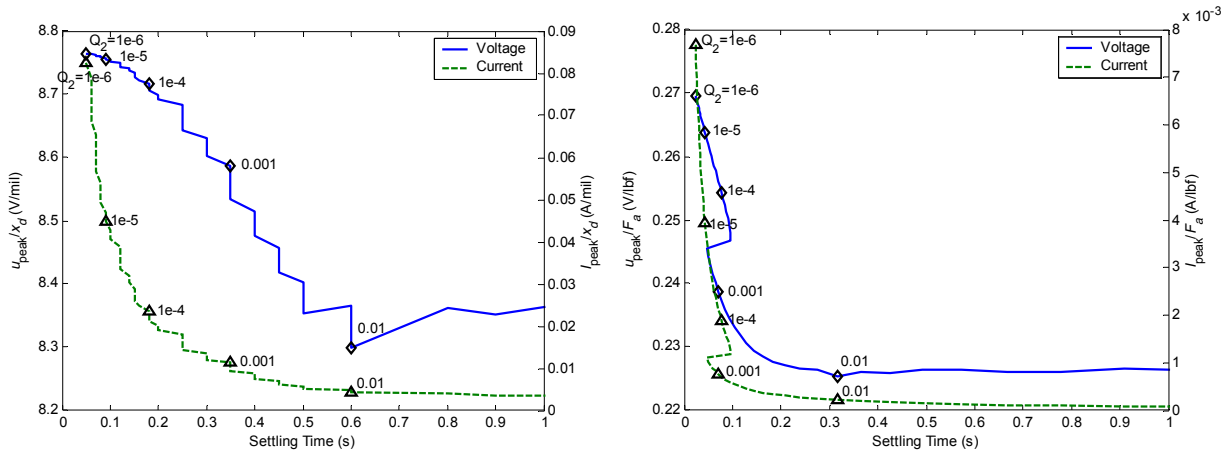
Table 3: Parameters for a PZN-PT piezo-crystal stack and amplifier.[19]

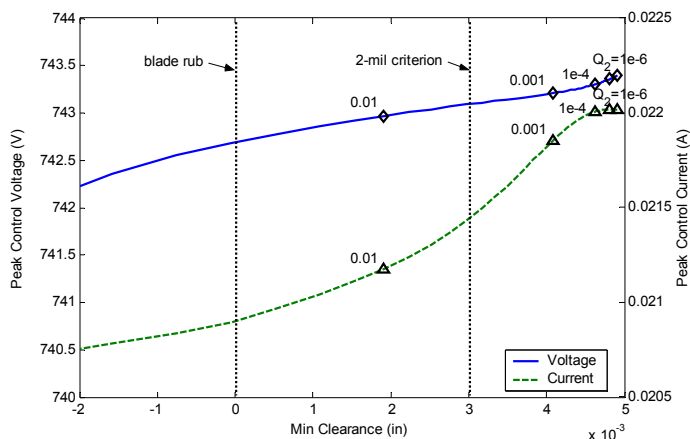| Property	Value	Property	Value
Piezoelectric coefficient d_{33}	7.87×10^{-8} in/V	Dielectric permittivity ε_{33}	1.13 nF/in
Number of wafers n	127	Rated current I_r	1 A
Modulus Y_{33}^E	1.21×10^6 psi	Rated voltage V_r	1000 V
Density ρ	0.296 lb/in³		

Figure 8: Piezoelectric actuator step response trade curves as functions of Q_2: (a) x_d disturbance, (b) F_a disturbance.

Controller Design

The LQG control law for the piezoelectric system was designed in a similar fashion to the servohydraulic actuator, however order reduction was not necessary because the system only consists of three states: position x_a, velocity $\dot{x}_a$, and stack voltage U. For the linear Kalman estimator design, it was heuristically assumed that the measurement and process noise covariances are identical to those in Section IV.

Results and Discussion

The open loop response of the stack exhibits a lightly damped resonance at 634 Hz, which is well above the Nyquist frequency with a FADEC update rate of 50 Hz. To address this issue, a 10-kHz sample rate was used instead, which is typical of any commercially available piezoelectric servocontroller and is thus a realistic alternative for controller implementation. The two plots in Fig. 8 illustrate step trade curves versus the normalized stack voltage and current. A distinctive quality of piezoelectrics is their low energy consumption and low power draw which, in turn, has an indirect but favorable effect on self-heating. As is evident in the figure, power consumption goes to zero as Q_2 increases, because slower response times demand less current. Even when a constant force bias on the actuator is present, at steady state conditions such as cruise, control power also remains at zero. Examining the case with takeoff transient disturbances (using disturbances identical to those used in Section IV), the minimum clearance trade curves shown in Fig. 9 confirms that the nominal FACC performance is acceptable. In spite of the high-bandwidth nature of these devices, it can be seen that the response curves are comparable with the servohydraulic actuator because of the extremely large capacitance required for this design. As

an example operating point, step responses for $Q_2 = 1 \times 10^{-6}$ (which results in a minimum clearance of 4.82 mils) are shown in Fig. 10. The position step response exhibits very little oscillation, which is a favorable characteristic of the control system. For the force disturbance case, transient oscillations cannot be abated by adjustment of controller gains, which is expected from a steady-state estimation error resulting from a deterministic exogenous disturbance. Of course, for low-magnitude events these oscillations are not anticipated to be problematic.

An assessment of the FACC system robustness was conducted next. The system noise was set to the values used to design the Kalman estimator and the parameters were varied between 10% and 500% of their

Figure 9: Piezoelectric actuator takeoff transient response trade curves as functions of Q_2.
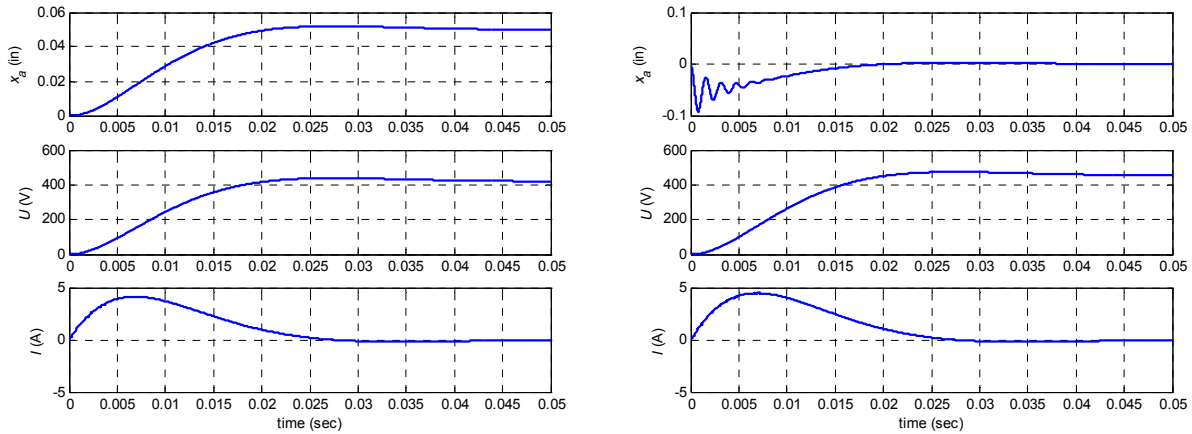
Figure 10: Piezoelectric actuator step responses with $Q_2 = 1 \times 10^{-6}$: (a) $x_d = 50$ mils, (b) $F_a = 2000$ lbf.

nominal values. As before, the simulation was evaluated with both takeoff transients and large-magnitude step disturbance inputs (see Fig. 10). The result of this evaluation is that, although the responses were perturbed slightly, instability in the system and violation of the 2-mil criterion did not occur throughout the test space. It can therefore be concluded that the piezoelectric control system exhibits excellent robustness characteristics to modeling uncertainty. From a performance perspective, the LQG controller can be designed such that the actuator's current draw is small, thus minimizing power consumption and self-heating and therefore making the stack less susceptible to depoling at high temperatures. However, the trade off between power consumption and performance must be respected: as the optimal controller gains are reduced, the propensity for blade rubs during transients increases.

VI.   Conclusions

In this paper, several requirements for a fast active clearance control system were identified for specific application to the high pressure turbine section. The design criteria used in this study were based on the requirements and constraints of a large commercial turbofan engine, particularly with regard to size, displacement, force, failsafe considerations, and power consumption. To satisfy the criteria for axisymmetric control, two systems were designed: one using electrohydraulic servovalve actuation and another using piezoelectric actuation. Servohydraulic devices are intended to fulfill immediate implementation needs, while piezoelectric actuation is expected to be reserved for a longer-term solution. It was shown that both actuation methods are feasible for FACC, although the underlying physics are remarkably different for each. Because of these differences, the closed loop response characteristics specific to each device must be given careful consideration before the controller is chosen. Those who design advanced clearance control systems can benefit from the observations made here because the present linear controller offers an insightful approach to select appropriate controller gains because the entire design process reduces to selection of a single parameter: the control effort weight. It is not the intent, however, to "single out" one of the two actuation schemes as a more suitable candidate for use in the present application.

Simulation results with the servohydraulic actuator showed that the LQG controller performed well in responding to step and takeoff transient disturbances on the shroud force and clearance. However, the performance of the system was severely degraded when the supply pressure was reduced, which may be alleviated by improving the controller's tolerance to faults. It was further shown that there exists not only a tradeoff between performance and control effort, but also one between performance and robustness. To improve robustness, one may opt to employ modern robust control techniques, such as variable structure (sliding mode) and H_∞ methods.

Using a similar control approach, the piezoelectric actuator designed with PZN-PT piezo-crystal material demonstrated adequate performance and robustness properties. Because control effort directly affects the power consumed to perform actuation, optimal control is an attractive control method for this device when the objectives are to maintain good efficiency and low self-heating. Piezoelectric materials have recently seen advancements in available strain, which can be amplified by mechanical means, but the major barriers for implementation are in their limited temperature capability and long-term durability in an engine environment. As further maturity and manufacturability in smart materials are realized, they may become feasible candidates for use in aircraft engines. Other than piezoelectrics, materials that show potential for FACC include shape memory alloys (Nitinol) and electrostrictive polymers (P[VDF – TrFE]).

References

[1] Lattime, S.B., Steinetz, B.M., "Turbine engine clearance control systems: current practices and future directions," *Proceedings of the 38th Joint Propulsion Conference and Exhibit*, AIAA-2002-3790, 2002.

[2] Wiseman, M.W., Guo, T., "An investigation of life extending control technologies for gas turbine engines," *Proceedings of American Control Conference*, 2001.

[3] Kawecki, E.J., "Thermal response turbine shroud study," Air Force Aero Propulsion Laboratory Technical Report AFAPL-TR-79-2087, 1979.

[4] Hailia, E., Lenahan, D., Thomas, T., "Energy efficient high pressure turbine test hardware detailed design report," NASA CR-167955, 1982.

[5] Kypuros, J.A., Melcher, K.M., "A reduced model for prediction of thermal and rotational effects on turbine tip clearance," NASA/TM-2003-212226, 2003.

[6] Melcher, K.M., Kypuros, J.A., "Toward a fast-response active turbine tip clearance control," *Proceedings of the International Symposium on Air Breathing Engines*, ISABE 2003-1102, 2003.

[7] Lattime, S.B., Steinetz, B.M., "Test rig for evaluating active turbine tip clearance control concepts," *Proceedings of the 39th Joint Propulsion Conference and Exhibit*, AIAA-2003-4700, 2003.

[8] Zeisberger, A., Eberl, J., Wenzl, J., "High temperature clearance measurements," *Proceedings of the International Symposium on Air Breathing Engines*, ISABE 2003-1144, 2003.

[9] MOOG, Inc., Jamison Rd., East Aurora, NY 14052, USA.

[10] Chopra, I., "Review of state of art of smart structures and integrated systems," *AIAA Journal*, Vol. 40, No. 11, 2003, pp. 2145-2187.

[11] Niezrecki, C., Brei, D., Balakrishnan, S., Moskalik, A., "Piezoelectric actuation: state of the art," *Shock and Vibration Digest*, Vol. 33, No. 4, 2001, pp. 269-280.

[12] Park, S.E., Shrout, T.R., "Ultrahigh strain and piezoelectric behavior in relaxor based ferroelectric single crystals," *J. Applied Physics*, Vol. 82, No. 4, 1997, pp. 1804-1811.

[13] Portloch, L.E., Schetky, L.M., Steinetz, B.M., "Shape memory alloy adaptive control of gas turbine engine blade tip clearance," *Proceedings of the 32nd Joint Propulsion Conference and Exhibit*, AIAA-96-2805, 1996.

[14] Merritt, H.E., *Hydraulic Control Systems*, John Wiley and Sons, NY, 1967.

[15] Skogestad, S., Postlethwaite, I., *Multivariable Feedback Control: Analysis and Design*, John Wiley and Sons, NY, 1996, pp. 352-362.

[16] Franklin, G.F., Powell, J.D., Workman, M.W., *Digital Control of Dynamic Systems*, 3rd Edition, Addison-Wesley, Menlo Park, 1998, p. 371.

[17] Prechtl, E.F., Hall, S.R., "Design of a high efficiency, large stroke electromechanical actuator," *J. Smart Materials and Structures*, Vol. 8, 1999, pp. 13-30.

[18] Chandrasekaran, S., Linder, D.K., "Power flow through controlled piezoelectric actuators," *J. Intelligent Material Systems and Structures*, Vol. 11, No. 6, 2000, pp. 469-481.

[19] TRS Ceramics, Inc., 2820 E. College Avenue, Suite J, State College, PA 16801, USA.

Appendix

Nomenclature Addendum

A_p	piston area	d_s	spool diameter
C_d	servovalve discharge coefficient	i	servovalve current
F_a	actuator load force	k_{fs}	spring constant for failsafe spring
G	sensitivity of servovalve spool position to driving current	k_{fl}	hydraulic fluid stiffness
		m	actuator assembly mass
I_r	servovalve rated current	p_1	pressure in servovalve chamber 1
K_{pq}	servovalve leakage coefficient	$\bar{p}_1$	$p_s/2$
L_c	servovalve coil inductance	p_2	pressure in servovalve chamber 2
q_1	volumetric flow rate of fluid entering servovalve chamber 1	$\bar{p}_2$	$2p_a$
		x_a	actuator position
q_2	volumetric flow rate of fluid entering servovalve chamber 2	x_s	servovalve spool position
		β	bulk modulus of hydraulic fluid
R_C	servovalve coil resistance	ρ	hydraulic fluid density
V	volume	τ	spool servocompensator time constant
c	actuator assembly damping		

Electrohydraulic Servovalve Model Development

   This section describes the development of the nonlinear servohydraulic actuator models and linearization assumptions used for the controller/estimator design. The forthcoming analysis is derived from Ref 14. Referring to Fig. 3, the net flow entering chamber #1 depends on the actuator velocity, the leakage induced by the chamber pressure, and the chamber fluid compliance, expressed as

$$q_1 = A_p \dot{x}_a + K_{pq} p_1 + \frac{A_p^2}{k_{fl}} \dot{p}_1 \tag{A.1}$$

where A_p is the piston area, K_{pq} is the leakage coefficient (here expressed as a linearized parameter), and k_{fl} is the fluid's bulk stiffness. This bulk stiffness is a function of the fluid's modulus β and the chamber volume V, as described by the following equation:[14]

$$k_{fl} = \frac{4\beta A_p^2}{V} \tag{A.2}$$

It is assumed that the chamber volumes and piston areas on either side of the actuator are identical. For this study, a k_{fl} of 2.2×10^6 lbf/in was used, representative of DTE-24 hydraulic fluid ($\beta = 150 \times 10^6$ psi). The fluid exiting chamber #2 is described by a similar equation in terms of the pressure p_2, and is expressed as follows:

$$q_2 = A_p \dot{x}_a - K_{pq} p_2 - \frac{A_p^2}{k_{fl}} \dot{p}_2 \tag{A.3}$$

The flow both into and out of the actuator are described by an orifice characteristic equation that accounts for resistive losses. The flow into chamber #1 is a function of the pressure drop across the orifice and the orifice size, which is piecewise about $x_s = 0$ assuming that the spool and orifice do not overlap or underlap at the null region:[14]

$$q_1^+(x_s, p_1) = C_d \pi d_s x_s \, \text{sgn}(p_s - p_1) \sqrt{\frac{2}{\rho}|p_s - p_1|}$$

(A.4)

$$q_1^-(x_s, p_1) = C_d \pi d_s x_s \, \text{sgn}(p_1 - p_a) \sqrt{\frac{2}{\rho}|p_1 - p_a|}$$

where it is apparent that $\pi d_s x_s$ is equivalent to the orifice area. The superscripts (+) and (–) denote the sign of x_s. Here, we assume that the valve is perfectly symmetric, so the flow coefficient C_d and the orifice areas are equal on both sizes of the valve. A similar relationship can be written for chamber #2 as

$$q_2^+(x_s, p_2) = C_d \pi d_s x_s \, \text{sgn}(p_2 - p_a) \sqrt{\frac{2}{\rho}|p_2 - p_a|}$$

(A.5)

$$q_2^-(x_s, p_2) = C_d \pi d_s x_s \, \text{sgn}(p_s - p_2) \sqrt{\frac{2}{\rho}|p_s - p_2|}$$

Direct substitution of Eqs. (A.4) and (A.5) into (A.1) and (A.3), respectively gives a piecewise representation of the coupling between spool position and supply pressure.

In order to couple the driving voltage to the actuator input flow, the dynamics of the coil and servocompensator must also be incorporated into the model. Those of the coil are introduced by relating the loop current to the load voltage by writing

$$u = L_c \frac{di}{dt} + R_c i$$

(A.6)

where L_c and R_c are the inductance and resistance of the coil, respectively. The time constant τ of the servocompensator is reported by most manufacturers, which relates current to spool position. This is modeled as

$$Gi = \tau \dot{x}_s + x_s$$

(A.7)

where G is the sensitivity between current and spool position.

The equation of motion for the actuator and shroud hangar completes the system model. These dynamics are incorporated by writing

$$m\ddot{x}_a + c\dot{x}_a + F_C \, \text{sgn}(\dot{x}_a) + k_{fs} x_a = (p_1 - p_2) A_p - F_a$$

(A.8)

Here, m is the combined mass of the shroud hangar and actuator rod, c is the viscous damping coefficient, k_{fs} is the stiffness of the failsafe return spring, F_C is the Coulomb friction force and F_a is the external shroud force. Eqs. (A.1) and (A.3) to (A.8) constitute the complete nonlinear model for the servohyrdaulic system.

The linear model was developed by assuming that $x_s > 0$ for all time in order for the system to be described by $q_1^+(x_s, p_1)$ and $q_2^+(x_s, p_2)$ only, $p_s > p_1$ and $p_2 > p_a$, and $F_C = 0$. Eqs. (A.4) and (A.5) were evaluated at assumed mean chamber pressures to eliminate the nonlinear dependence on flow. To this end, p_1 and p_2 were heuristically linearized about $\bar{p}_1 = p_s/2$ and $\bar{p}_2 = 2p_a$, respectively. Eqs. (A.4) and (A.5) may then be substituted into Eqs. (A.1) and (A.3) as follows:

$$C_d \pi d_s x_s \sqrt{\frac{2}{\rho}(p_s - \bar{p}_1)} = A_p \dot{x}_a + K_{pq} p_1 + \frac{A_p^2}{k_{fl}} \dot{p}_1$$

(A.9)

$$C_d \pi d_s x_s \sqrt{\frac{2}{\rho}(\bar{p}_2 - p_a)} = A_p \dot{x}_a - K_{pq} p_2 - \frac{A_p^2}{k_{fl}} \dot{p}_2$$

(A.10)

The state space representation is formed by populating the state vector as $x = \{x_a \quad \dot{x}_a \quad p_1 \quad p_2 \quad x_s \quad i\}^T$, then writing out Eqs. (A.9) to (A.13) in matrix form. The state space matrices are

$$A = \begin{bmatrix}
0 & 1 & 0 & 0 & 0 & 0 \\
-\dfrac{k_{fs}}{m} & -\dfrac{c}{m} & \dfrac{A_p}{m} & -\dfrac{A_p}{m} & 0 & 0 \\
0 & -\dfrac{k_{fl}}{A_p} & -\dfrac{k_{fl}K_{pq}}{A_p^2} & 0 & \dfrac{k_{fl}C_d\pi d_s}{A_p^2}\sqrt{\dfrac{2}{\rho}(p_s - \overline{p}_1)} & 0 \\
0 & \dfrac{k_{fl}}{A_p} & 0 & -\dfrac{k_{fl}K_{pq}}{A_p^2} & -\dfrac{k_{fl}C_d\pi d_s}{A_p^2}\sqrt{\dfrac{2}{\rho}(\overline{p}_2 - p_a)} & 0 \\
0 & 0 & 0 & 0 & -\dfrac{1}{\tau} & \dfrac{G}{\tau} \\
0 & 0 & 0 & 0 & 0 & -\dfrac{R_c}{L_c}
\end{bmatrix} \tag{A.11}$$

$$B = \begin{bmatrix} 0 & 0 & 0 & 0 & 0 & \dfrac{1}{L_c} \end{bmatrix}^T \tag{A.12}$$

$$F = \begin{bmatrix} 0 & \dfrac{1}{m} & 0 & 0 & 0 & 0 \end{bmatrix}^T \tag{A.13}$$

$$C = \begin{bmatrix} 1 & 0 & 0 & 0 & 0 & 0 \end{bmatrix} \tag{A.14}$$

and $D = 0$.

REPORT DOCUMENTATION PAGE

1. AGENCY USE ONLY (Leave blank)	2. REPORT DATE	3. REPORT TYPE AND DATES COVERED
	July 2004	Technical Memorandum

4. TITLE AND SUBTITLE

A Study on the Requirements for Fast Active Turbine Tip Clearance
Control Systems

5. FUNDING NUMBERS

WBS–22–714–70–08

6. AUTHOR(S)

Jonathan A. DeCastro and Kevin J. Melcher

7. PERFORMING ORGANIZATION NAME(S) AND ADDRESS(ES)

National Aeronautics and Space Administration
John H. Glenn Research Center at Lewis Field
Cleveland, Ohio 44135–3191

8. PERFORMING ORGANIZATION REPORT NUMBER

E–14615

9. SPONSORING/MONITORING AGENCY NAME(S) AND ADDRESS(ES)

National Aeronautics and Space Administration
Washington, DC 20546–0001

10. SPONSORING/MONITORING AGENCY REPORT NUMBER

NASA TM—2004-213121
AIAA–2004–4176

11. SUPPLEMENTARY NOTES

12a. DISTRIBUTION/AVAILABILITY STATEMENT

Unclassified - Unlimited
Subject Category: 07   Distribution: Nonstandard

Available electronically at http://gltrs.grc.nasa.gov

This publication is available from the NASA Center for AeroSpace Information, 301–621–0390.

12b. DISTRIBUTION CODE

13. ABSTRACT (Maximum 200 words)

This paper addresses the requirements of a control system for active turbine tip clearance control in a generic commercial turbofan engine through design and analysis. The control objective is to articulate the shroud in the high pressure turbine section in order to maintain a certain clearance set point given several possible engine transient events. The system must also exhibit reasonable robustness to modeling uncertainties and reasonable noise rejection properties. Two actuators were chosen to fulfill such a requirement, both of which possess different levels of technological readiness: electrohydraulic servovalves and piezoelectric stacks. Identification of design constraints, desired actuator parameters, and actuator limitations are addressed in depth; all of which are intimately tied with the hardware and controller design process. Analytical demonstrations of the performance and robustness characteristics of the two axisymmetric LQG clearance control systems are presented. Takeoff simulation results show that both actuators are capable of maintaining the clearance within acceptable bounds and demonstrate robustness to parameter uncertainty. The present model-based control strategy was employed to demonstrate the tradeoff between performance, control effort, and robustness and to implement optimal state estimation in a noisy engine environment with intent to eliminate ad hoc methods for designing reliable control systems.

14. SUBJECT TERMS

Clearances; Turbines

15. NUMBER OF PAGES

23

16. PRICE CODE

17. SECURITY CLASSIFICATION OF REPORT	18. SECURITY CLASSIFICATION OF THIS PAGE	19. SECURITY CLASSIFICATION OF ABSTRACT	20. LIMITATION OF ABSTRACT
Unclassified	Unclassified	Unclassified	